Spin polarization of ^{27}Na and ^{31}Al in intermediate energy projectile fragmentation of ^{36}S

D. Borremans,[1] J. M. Daugas,[1,*] S. Teughels,[1] D. L. Balabanski[1,2] N. Coulier,[1] F. de Oliveira Santos,[3] G. Georgiev,[1,†] M. Hass,[4] M. Lewitowicz,[3] I. Matea,[3] Yu. E. Penionzhkevich,[5] W.-D. Schmidt-Ott,[6] Yu. E. Sobolev,[5] M. Stanoiu,[3] K. Vyvey,[1] and G. Neyens[1]

[1]*Instituut voor Kern- en Stralingsfysica, KU Leuven, Celestijnenlaan 200D, B-3001 Leuven, Belgium*
[2]*Saint Kliment Ohridski University of Sofia, Bg-1164 Sofia, Bulgaria*
[3]*GANIL, Boîte Postale 55027, F-14076 Caen Cedex 5, France*
[4]*The Weizmann Institute, Il-76100 Rehovot, Israel*
[5]*FLNR-JINR, Department of Physics, Ru-141980 Dubna, Russia*
[6]*Zweites Physikalisches Institut, Universität Göttingen, D-37077 Göttingen, Germany*

(Received 9 August 2002; published 1 November 2002)

Spin-polarized ^{27}Na and ^{31}Al secondary beams have been produced at GANIL by the fragmentation of a 77.5 MeV/nucleon $^{36}S^{16+}$ primary beam onto a ^{9}Be target. The primary beam was deflected at an angle of $-2(1)°$ with respect to the entrance of the LISE3 spectrometer, where the target was placed. For linear momenta higher than that of the ^{36}S projectiles, a deduced spin polarization $P=-6.2(9)\%$ and $P=-1.5(4)\%$ was obtained for ^{27}Na and ^{31}Al projectile fragments. These results demonstrate for the first time that fragments far from the projectile mass can be substantially polarized.

DOI: 10.1103/PhysRevC.66.054601 PACS number(s): 24.70.+s, 25.70.−z, 21.10.−k, 23.40.−s

I. INTRODUCTION

Spin-oriented nuclear ensembles are needed for a variety of physics experiments, e.g., to investigate the structure of nuclei by measuring their static nuclear moments, for fundamental interaction studies, etc. Several methods with their own specific range of applicability, depending on the production method and element of interest, have been developed to polarize nuclear ensembles at low-energy ISOL-type beams [1–4]. The possibility to produce spin polarization of a nuclear ensemble via projectile-fragmentation reactions at intermediate energies [5,6] gives the opportunity to investigate the structure of exotic nuclei and in particular of neutron-rich nuclei in in-flight experiments. Up to now, spin-polarized secondary beams have been used to measure static nuclear moments of ^{12,13,14,15,17}B [6,7], ^{17}N [8], and ^{32}Cl [9]. A systematic study of the fragment polarization as a function of the longitudinal momentum distribution has been done in Ref. [6] for ^{12,13}B fragments which are produced in the fragmentation of ^{14,15}N beams on different targets (^{197}Au,^{93}Nb, and ^{27}Al). In all these studies the secondary beam differs only by two or three nucleons from the primary beam. Okuno *et al.* developed a kinematical model, based on the Goldhaber abrasion/ablation model for high-energy fragmentation [5,6] to explain the qualitative behavior of the polarization as a function of fragment linear momentum. For the reactions on the ^{197}Au and ^{93}Nb targets, the polarization is overestimated by a factor of 4, while for the reaction on a ^{27}Al target, where the nuclear attraction is expected to be the dominant process in the reaction mechanism, theory and experiment differ by a factor of 10. The present study addresses the issues of spin-polarization for reactions with a very light target (e.g., ^{9}Be) and with the secondary beam differing significantly from the primary one. Since at present we lack a detailed understanding of the process, more experimental studies are needed to trace the trends and provide a firm basis for the theoretical analysis. In this work, pure secondary beams of ^{27}Na and ^{31}Al were produced in the fragmentation of ^{36}S nuclei on a ^{9}Be target. Note that, e.g., in the case of ^{27}Na, 25% of the projectile nucleons are abraded. We investigated the spin-polarization of these secondary beams, using the β-nuclear magnetic resonance (β-NMR) technique [10]. It was for the first time that spin-polarized fragment beams were produced at the GANIL facility.

II. POLARIZATION IN A PROJECTILE-FRAGMENTATION REACTION

The projectile-fragmentation reaction can produce exotic isotopes in every mass region, both at the proton and neutron-rich side of the nuclear chart [11]. Several qualitative models [12–15] are able to reproduce the characteristic features, such as the momentum distribution, of nuclei produced in such reactions. At relativistic energies the fragmentation process occurs for peripheral collisions. One can assume that nucleons from the projectile, which belong to the geometrical overlapping volume with the target nuclei, are removed and the rest of the projectile, called ejectile or prefragment, follows its way with a velocity similar to that of the primary beam. This simple picture, known as the ''participant-spectator model,'' results in a Gaussian-like shape for the longitudinal momentum distribution of the outgoing fragments. The width of this distribution depends on the fragment and projectile mass and is known as the Goldhaber width $\sigma=\sigma_0\sqrt{[A_f(A_p-A_f)]/A_p-1}$ with $\sigma_0=80$ MeV/c [6,12]. The reaction mechanism is not so simple at intermediate energies because of the interplay between transfer and fragmentation reactions [16,18]. In first approxi-

*Present address: CEA/DIF/DPTA/PN, BP 12, F-91680 Bruyeres le Chatel, France.

†Present address: GANIL, BP 55027, F-14076 Caen Cedex 5, France.

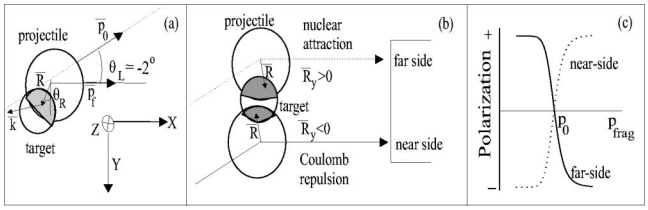

FIG. 1. (a),(b) Schematic view of the definition of the used orientation frame and the trajectories of the fragment and projectile nuclei. $\vec{p}_0$ and $\vec{p}_f$ are the linear momentum of the projectiles and fragments, respectively, while $\vec{k}$ is the linear momentum of the removed nucleons. The position of the removed nucleons is presented by $\vec{R}$ and θ_R [6]. (b) Schematic view of the near-side/far-side trajectories of the fragment and projectile nuclei. In the far-side trajectory, nuclear attraction dominates while in the near-side trajectory Coulomb repulsion dominates. (c) Simulation of polarization in the kinematical model of Okuno *et al.* [6] for an example of a near-side and a far-side trajectory of the projectile nuclei.

mation one can assume that fragmentation is the dominant process [19] using the mentioned participant-spectator model. Asahi *et al.* demonstrated experimentally that projectile fragments can be polarized when emitted at a finite angle θ_L and explained it in the framework of this model, considering the abraded nucleons as participants and the fragment as a spectator [5]. Conservation of linear and angular momentum (spin) in the projectile-rest frame gives (assuming zero spin of the projectile, a static target and negligible intrinsic spins of the removed nucleons)

$$\vec{p}_f=\vec{p}_0-\vec{k}, \quad \vec{J}_f=-\vec{R}\times\vec{k}, \quad \text{and} \quad \vec{J}_z=(R_y k_x-R_x k_y)\vec{u}_z \tag{1}$$

with $\vec{p}_f$, $\vec{p}_0$, and $\vec{k}$ the linear momenta of the fragment, the projectile and the abraded nucleon(s), respectively, $\vec{J}_f$ the angular momentum of the fragment. $\vec{R}$ is the position vector of the removed nucleon(s) [Fig. 1(a) and Ref. [6]]. We define a reference frame with the x axis parallel to the fragment beam-axis and the Z axis along $\vec{p}_0\times\vec{p}_f$, such that the polarization is defined as positive when parallel to Z. The indices x,y,z indicate the projection on these axes. The linear momentum $\vec{p}_f$ of the fragment, with a Gaussian distribution around $\vec{p}_0$ and a finite Goldhaber width σ [12], is correlated with its angular momentum $\vec{J}_f$ via $\vec{k}$, the linear momentum of the abraded nucleon(s). With the assumption of uniform removal of the nucleons over the overlap region of the projectile and the target, we get a mean $\overline{R}_x=0$ and $|\overline{R}_y|=R_0$, the radius of the projectile. For a certain fragment momentum $\vec{p}_f$ the resulting polarization is $P=\overline{J}_z/J_f=\overline{R}_y k_x/J_f$. In the center of the fragment momentum distribution ($p_f=p_0$), $\vec{k}$ is perpendicular to $\vec{p}_0$, resulting in $k_x=0$ and thus a zero polarization. The average value of $\overline{R}_y$ is positive or negative depending on which process—nuclear attraction or Coulomb repulsion—dominates the fragmentation reaction. For a near-side trajectory [Fig. 1(b)], that is dominated by Coulomb repulsion, $\overline{R}_y$ is negative. In that case we find a positive polarization for fragments with a higher momentum ($p_f>p_0$) and a negative polarization for fragments moving slower than the primary beam [Fig. 1(c)]. For a far-side trajectory, dominated by nuclear attraction, $\overline{R}_y$ is positive [Fig. 1(b)] and an opposite behavior for the polarization as a function of the fragment momentum p_f is seen.

In general both the Coulomb repulsion (near-side) and nuclear attraction (far-side) processes can occur in the fragmentation reaction. That means the assumption of uniform nucleon removal is not valid. In that case $\overline{R}_x$ is not necessarily zero such that in the polarization $P=\overline{J}_z/J_f=\overline{R}_y k_x-\overline{R}_x k_y/J_f$ the extra term $-\overline{R}_x k_y$ leads to a vertical and horizontal shift of the polarization curve as a function of p_f. Consequently the polarization is no longer vanishing for $p_f=p_0$. In this case, the average position of the removed nucleons $\vec{R}$ is not parallel with the y axis, indicating a shift of the averaged position of the removed nucleons essentially due to rescattering effects [6]. The angle θ_R between $\vec{R}$ and the y axis, which determines the size of $\overline{R}_x$, can be calculated only approximately with an intranuclear cascade model [20], including nucleon-nucleon cross sections, secondary reactions and the Pauli-blocking effect [21]. In the polarization model of Okuno *et al.*, the reaction angle θ_R is introduced as a free parameter.

III. PRODUCTION OF POLARIZED FRAGMENTS AT GANIL

For the production of the secondary ^{27}Na/^{31}Al beam, a 1 mm thick ^{9}Be target and a $^{36}S^{16+}$ ion primary beam at 77.5 MeV/nucleon were used. The outgoing fragments were selected by their mass over charge ratio through the LISE3 spectrometer by two dipoles, a Be wedge-degrader placed at the dispersive plane after the first dipole. An extra purification is performed by a Wien-filter [11]. This filter consists of a static magnetic field B_{Wien} in the horizontal direction and a perpendicular electric field to select the nuclei by their velocity. The unambiguous identification of the fragments and of the purity of the secondary beam was achieved by energy-loss and time of flight measurements using a removable Si detector. The purity of the secondary beam varied from 93% to 98% for ^{27}Na and from 97% to 99% for ^{31}Al, depending on the selected momentum window. The Si detector was taken out of the beam after the ion identification. The presence of a position sensitive Si detector (500 μm) inside the implantation chamber allowed event-by-event verification of the purity and the position of the secondary beam.

To create spin polarization, the primary beam was deviated by 2° via a movable dipole magnet [Fig. 2(a)]. This dipole magnet can deflect the primary beam from 0° up to $-3.5°$ with an angular acceptance of 1°. The fragments were selected at an angle $\theta_L=-2(1)°$.

Slits in the horizontal dispersive plane controlled the longitudinal momentum acceptance window. We put $(\Delta p/p)(^{27}\text{Na})=\pm 0.29\%$ and $(\Delta p/p)(^{31}\text{Al})=\pm 0.46\%$. To select another part of the momentum distribution, we changed the target thickness by tilting the target over an angle θ_t. An

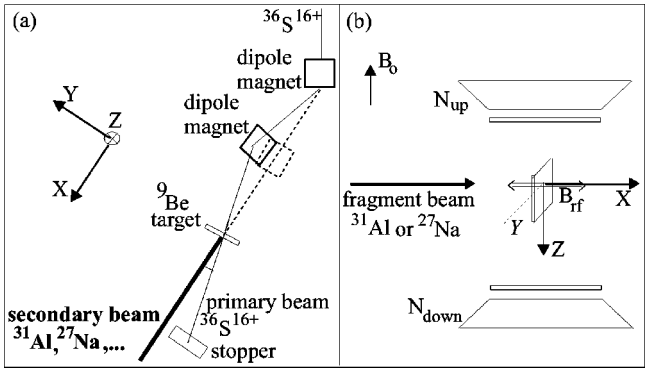

FIG. 2. Experimental setup for the study of spin polarization of secondary beams in in-flight experiments at GANIL. (a) Schematic view of a part of the LISE beam line, indicating the beam deflection via the movable dipole. (b) Schematic view of the experimental setup, where the secondary beam was analyzed.

increase of the target thickness corresponds to a decrease of the outgoing fragment linear momentum. Keeping the same magnetic rigidity $B\rho$ for the dipoles of the spectrometer, we were able to investigate the momentum distribution of the produced fragments for several momentum cuts in the high-energy part of the momentum distribution. The theoretical production yield and $B\rho$ values corresponding to particular target thicknesses have been obtained using the LISE program with the convolution of a gaussian and an exponential shape [16,17]. The calculated yield was scaled to the maximum of the experimental yield. This longitudinal momentum selection was experimentally verified by measuring the selected fragment intensity for different target thicknesses, i.e., with an angle θ_t on the target of 40°, 50°, and 58° for ^{27}Na and of 50° and 56° for ^{31}Al (Fig. 3). After the selection, the nuclei were decelerated by an Aluminum sheet of 1500 μm that was positioned in a degrader box in front of the experimental β-NMR vacuum chamber. In this manner, the nuclei obtained the right energy to be implanted in a NaCl or MgO crystal of 2 mm thickness. In Fig. 2(b), a scheme of the experimental setup is presented.

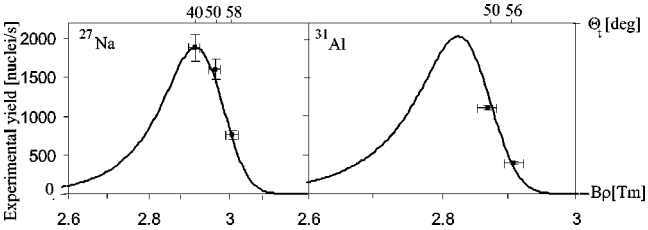

FIG. 3. Experimental yields of ^{27}Na and ^{31}Al fragments as a function of the calculated magnetic rigidity $B\rho$ (lower scale), which is related to the effective target thickness (varied by tilting the target over an angle θ_t, upper scale). The theoretical yield distribution is obtained from the LISE program, assuming a Gaussian curve with an exponential tail [16,17].

IV. EXPERIMENTAL DETERMINATION OF REACTION-INDUCED POLARIZATION *P*

A. Experimental procedure: β-NMR

The ^{27}Na and ^{31}Al fragments were continuously implanted at room temperature in a NaCl or a MgO single crystal, respectively, both having a fcc lattice structure. The crystal was positioned between the poles of an electromagnet, which produces a magnetic field B_0, antiparallel to Z [Fig. 2(b)]. Additionally, a linearly polarized oscillating magnetic field B_{rf} was applied, oriented perpendicular to B_0. This radio-frequent (rf) field B_{rf} breaks the axial symmetry of the Hamiltonian. When the Larmor precession ν_L of the nuclear spins matches the radio frequency ν_{rf}

$$\nu_L = \frac{g\mu_N B_0}{h} = \nu_{rf} \tag{2}$$

the initial polarization is destroyed. This can be detected by a change of the asymmetry of the nuclear β decay, $R = N_{up}/N_{down}$, as a function of the rf-frequency ν_{rf} (keeping the static magnetic field strength B_0 constant) or vice versa. N_{up} and N_{down} are the coincident count rates in the telescope detectors above and below the crystal, respectively [Fig. 2(b)]. In this experiment, the static magnetic field strength B_0 was the variable parameter and the rf frequency was fixed. This field strength was varied in regular time intervals of a few minutes and monitored with a Hall probe on an event-by-event basis. The rf frequency was swept continuously around a fixed value ν_{rf} over a range $\nu_{rf}-\Delta\nu_{rf}$ to $\nu_{rf}+\Delta\nu_{rf}$. This was done because the exact resonance frequency was not known (at least not for ^{31}Al) prior to this experiment and we aimed for maximum destruction of polarization. The modulation range $2\Delta\nu_{rf}$ was scanned with a modulation frequency of 50 Hz and a rf-field strength of 6–10 G, using a RAMP scan profile in which the frequency is varied linearly from $\nu_{rf}-\Delta\nu_{rf}$ to $\nu_{rf}+\Delta\nu_{rf}$ and changes then abrupt to $\nu_{rf}-\Delta\nu_{rf}$. Because of the particular shape of the modulation profile, the amount of β asymmetry being destroyed at a resonant rf signal can be expected to be the same for the entire modulation interval. More details about the experimental setup and procedure can be found in Ref. [22].

B. Determination of *P*

The resonant magnetic field strength $B_{0,r}$ and the value of the rf frequency $\nu_{rf}\pm\Delta_{rf}$ determine the g factor of the nuclear state using Eq. (2) [10]. The difference in β asymmetry in and out of resonance determines the polarization of the nuclear ensemble.

The angular distribution of β decay is given by [23]

$$W(\theta,\phi,\tau) = \sqrt{4\pi}\,\frac{v}{c}\sum_{k,n} A_k Q_k^n B_k^n(I,\tau) Y_k^n(\theta,\phi) \tag{3}$$

with θ,ϕ the angles defining the detector position with respect to the chosen reference frame (as in Figs. 1 and 2). A_k are the radiation parameters determined by the type of radia-

tion. $B_k^n(I,\tau)$ is the time-integrated orientation tensor for a nuclear ensemble with lifetime τ (odd k tensor components are related to the amount of polarization, even ones to the amount of alignment). Q_k^n represent the experimental losses of orientation between the time of production and detection. v is the velocity of the β particles and c denotes the constant speed of light.

Since for allowed β-decay $A_k \neq 0$ for odd k only and because A_k decreases strongly for high k values [2] and the higher order terms of B_k^n are negligible for $I \leqslant 4\hbar$ [24], we can restrict expression (3) to $k=1$. Because of the axial symmetry of the experimental setup, only $n=0$ terms contribute to the final angular distribution

$$W(\theta,\tau) = 1 + \frac{v}{c} A_1 Q_1 B_1^0(I,\tau)\cos\theta. \tag{4}$$

The spin-orientation of the nuclear ensemble will be perturbed by the two magnetic interactions. This perturbation is expressed by the perturbation factors $G_{kk'}^{nn'}(\nu_L,\nu_{rf},\tau)$, which in case of a NMR-interaction reduces to terms with $k=k'$ and $n=n'$ [10]

$$\begin{aligned} B_1^0(I,\tau) &= \sum_{k',n'} G_{1k'}^{0n'}(\nu_L,\nu_{rf},\tau) B_{k'}^{n'}(I,t=0) \\ &= G_{11}^{00}(\nu_L,\nu_{rf},\tau) B_1^0(I,t=0) \end{aligned} \tag{5}$$

with $B_1^0(I,t=0)$ the tensor component describing the reaction induced polarization $P(t=0)$ with respect to the Z axis [23]

$$B_1^0(I,t=0) = -\sqrt{\frac{3I}{I+1}} P(t=0). \tag{6}$$

It can be shown that in the resonance condition, with a sufficiently strong rf field, all Zeeman levels are equally populated, i.e., $G_{11}^{00}(\nu_L=\nu_{rf})=0$. At resonance the reaction-induced polarization is then destroyed and we find an isotropic angular distribution, derived from Eqs. (4) and (5): $W(\theta,\tau)=1$ for all θ. Far from the resonance condition, the rf perturbation is negligible or $G_{11}^{00}(\nu_L \neq \nu rf)=1$, so the measured β-asymmetry reflects the initial polarization. The experimental ratio

$$R(B_0) = \frac{N_{up}}{N_{down}} = \frac{\epsilon_{up} W(180°)}{\epsilon_{down} W(0°)} \tag{7}$$

is measured as a function of the static magnetic field strength B_0, as shown in Fig. 4. Here $\epsilon_{up}/\epsilon_{down}$ represents an experimental correction factor, the experimental asymmetry due to the possible different efficiencies of the detectors, the position of the beam with respect to the crystal, etc. To extract out of these data the polarization, independent of this experimental asymmetry $\epsilon_{up}/\epsilon_{down}$, the ratio out of resonance (R_{out}) which is sensitive to P, is compared to the ratio in resonance (R_{in}) which is sensitive to the experimental asymmetry of the detection setup

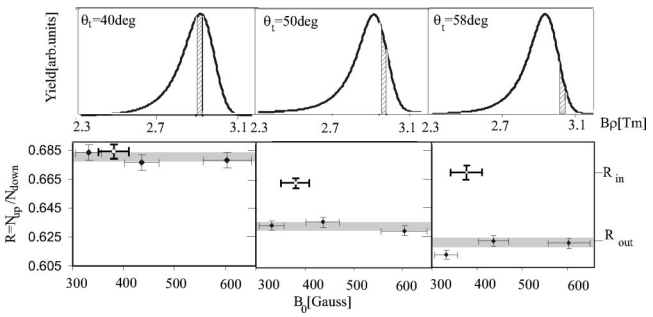

FIG. 4. (Top) Momentum selection of ^{27}Na corresponding to the different angles of the target. (Bottom) Experimental β asymmetries for the selected momentum windows. Notice that the resonant point (indicated in bold) equals the experimental β asymmetry with non-polarized nuclei. The β asymmetry of the points out of resonance is a measure for the reaction-induced polarization.

$$R_{in}(B_0 = B_{0,r}) = \frac{\epsilon_{up}}{\epsilon_{down}},$$

$$R_{out}(B_0 \neq B_{0,r}) = \frac{\epsilon_{up}}{\epsilon_{down}} \frac{1 - \frac{v}{c} A_1 Q_1 B_1^0(I,t=0)}{1 + \frac{v}{c} A_1 Q_1 B_1^0(I,t=0)}. \tag{8}$$

The experimental asymmetry cancels when we take the normalized ratio $R_n = R_{out}/R_{in}$. In order to extract the polarization P created in the projectile-fragmentation reaction out of the measured normalized β asymmetry R_n, we calculate

$$\frac{R_n - 1}{R_n + 1} = -\frac{v}{c} A_1 Q_1 B_1(I,t=0) = \sqrt{\frac{3I}{I+1}} \frac{v}{c} A_1 Q_1 P(t=0). \tag{9}$$

The factors v/c, A_1 and Q_1 determine how much of the reaction-induced polarization is experimentally measurable. The radiation parameter A_1 is related to the spins of the initial and final states of the β decay and depends on the kind of transition, Gamov-Teller or Fermi, β^+ or β^- [25]. Based on the observed decay schemes [26], the radiation parameters are calculated to be $A_1(^{27}\text{Na}) = 0.619$ and $A_1(^{31}\text{Al}) = 0.639$. The mean β energy for ^{31}Al ($E_\beta^M = 3.8$ MeV) and ^{27}Na ($E_\beta^M = 4.3$ MeV) is high such that $v/c = 0.99$, giving a minor reduction. Q_1 represents the experimental losses of the orientation. Before the implantation of the nuclei, spin polarization can be lost due to electron pickup of the fully stripped nuclei ^{31}Al and ^{27}Na passing through the material in the LISE beamline (wedge, Al-degrader, position sensitive Si detector) down to the stopper. Calculations with the LISE program for ^{27}Na and ^{31}Al ions in this energy range predict an electron pickup of less than one percent, inducing no loss of orientation. During their passage through the Wien-filter, the nuclear spins rotate over a small angle with the Larmor frequency [Eq. (2)]. In this experiment the field was set to $B_{Wien} = 252$ G. With the speed of the fragments of 10.14 cm/ns and 5 m effective magnetic length of the filter, the passage takes $t = 49$ ns. The spins or thus the polarization

symmetry axis Z, will be rotated over $\theta=\omega_L t$ around $\vec{B}_{Wien}$, causing a reduction of the measured spin polarization in the vertical direction. The reduction is minor and similar for both ^{31}Al and ^{27}Na: $\cos\theta=0.996$. After implantation and decay of the nuclei, the emitted β particles can scatter in the setup and the detectors. Also the solid angle of the detection setup needs to be taken into account. Both are calculated using a GEANT [27] simulation of the setup, resulting in a geometric factor $Q_{GEANT}=0.71(5)$ for the ^{27}Na nuclei implanted in a NaCl crystal and $Q_{GEANT}=0.80(3)$ for the ^{31}Al nuclei implanted in a MgO crystal. Besides this quantified losses which amount in total to $Q_1(^{27}\mathrm{Na})=0.70(5)$ and $Q_1(^{31}\mathrm{Al})=0.79(3)$, there are some uncontrolled orientation losses, due to the impurity of the crystal and possible implantation sites that may be perturbed for some of the nuclei. As we can not quantify them, we take these effects into account by a scaling factor ($q<1$) between the deduced polarization P and the reaction induced polarization $P=qP_r$. Taking into account all above effects we find for the deduced polarization

$$P\left(^{27}\mathrm{Na}, I=\frac{5}{2}\right)=1.59(6)\,\frac{R_n-1}{R_n+1}, \tag{10}$$

$$P\left(^{31}\mathrm{Al}, I=\frac{5}{2}\right)=1.37(4)\,\frac{R_n-1}{R_n+1}. \tag{11}$$

C. Results

The known ground state properties of ^{27}Na [$I^\pi=5/2^+$, $g=1.558(2)$, $t_{1/2}=301$ ms, $Q_\beta=9.010$ MeV] [28] fix the resonant magnetic field strength $B_{0,r}=436$ G for the rf settings $\nu_{rf}=450\pm35$ kHz, $\nu_{mod}=100$ Hz and $B_{rf}=4.5(1.5)$ G. The amount of induced polarization was measured for three different linear momentum windows of the nuclei with an acceptance $\Delta p/p=\pm0.29\%$. The first momentum cut in the outer wing of the yield distribution, corresponding to a target tilted at $\theta_t=58°$ (Fig. 4 top) showed a change in β asymmetry of $R_n=0.924$ or a reaction-induced polarization of minimal $P=-6.2(9)\%$. For nuclei selected in the center of the momentum distribution, the experimental polarization is found to be zero within the experimental precision. The measured and deduced spin polarizations are presented in Table I (top) for the different momentum cuts.

On ^{31}Al [$I^\pi=5/2^+$, $g=1.517(20)\,\mu_N$, $t_{1/2}=644$ ms, $Q_\beta=7.995$ MeV] [22] we performed measurements with two different momentum selections [Fig. 3(b)] with an acceptance of $\Delta p/p=\pm0.46\%$ and rf settings $\nu_{rf}=1000\pm12$ kHz, $\nu_{mod}=50$ Hz, $B_{rf}=10.0(1.5)$ G. The resonance field was found to be $B_{0,r}=859$ G from which the ^{31}Al factor of g could be deduced [22]. The change in β asymmetry was equal, within errors, for both momentum windows (Table I bottom), which is expected as both momentum cuts are far in the outer wing of the fragment momentum distribution. A polarization of $P=-1.5(4)\%$ was deduced.

Despite the use of the same target ^{9}Be and primary ^{36}S beam and the closeness in mass of both nuclei ^{27}Na and ^{31}Al, there is a large difference in the evaluated polarization, which will be discussed in the following section.

TABLE I. Polarization of the ^{27}Na and ^{31}Al nuclei, created in the projectile-fragmentation reaction of ^{36}S on ^{9}Be for different selections in the momentum distribution.

Angle target (deg)	Corresponding $B\rho$ (Tm)	Selected ion rate (ion/s)	Observed asymmetry R_n-1	Deduced polarization P (%)
1) **^{27}Na**				
40	2.915	1880	−0.007(8)	−0.6(7)
50	2.952	1601	−0.044(5)	−3.5(5)
58	3.025	755	−0.076(9)	−6.2(9)
2) **^{31}Al**				
56	2.865	457	−0.019(3)	−1.3(2)
50	2.910	1254	−0.022(6)	−1.5(4)

V. DISCUSSION

We compare the obtained polarizations with the calculations in the kinematical fragmentation model of Okuno *et al.* [5,6]. The parameters used in the calculation are the impact parameter b, the density of the projectile nucleus $\rho_i(b)$, the experimental deflection angle of the primary beam $\theta_L[=-2(1)°]$ and the reaction angle θ_R (Fig. 1). The impact parameter b is calculated to be $b(^{27}\mathrm{Na})=5.21(8)$ fm and $b(^{31}\mathrm{Al})=5.72(6)$ fm such that the geometrical overlapping volume corresponds to the number of abraded nucleons, assuming one evaporated nucleon per two abraded nucleons [18]. The density of the projectile nucleus $^{36}S^{16+}$ at a distance b of the nuclear center can be written in the Coulomb-modified Glauber model as $\rho_i(b)=\rho_i(0)\exp(-b^2/a_i^2)$ with the central nuclear density $\rho_i(0,^{36}S)=0.64$ fm^{-3} and the width of the density distribution $a_i(^{36}S)=2.40$ fm [29].

In Figs. 5(a) and 5(b), the experimental results for ^{27}Na

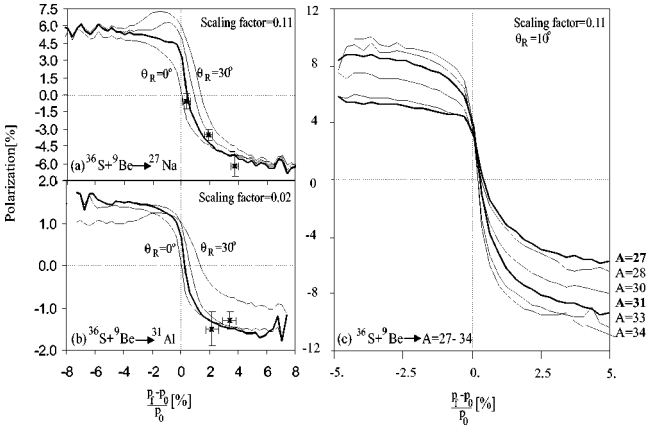

FIG. 5. (a),(b) Kinematical fragmentation model calculation of the reaction-induced polarization compared to the experimental data for ^{27}Na and ^{31}Al. The theoretical values overestimate the experimental ones by the mentioned scaling factors. (c) Comparison of calculated polarizations for fragments with mass $A=34$ down to $A=27$, produced in the fragmentation of a $A=36$ beam at 77.5 MeV/nucleon.

and ^{31}Al fragments are compared with the theoretical calculations. Note that the shape of the polarization curve as a function of the fragment linear momentum corresponds to that of a far-side trajectory, as we expect for light targets where nuclear attraction is the dominating process. In the calculations, the reaction angle θ_R, indicating the average position of the removed nucleons, is varied from 0° to 30° with steps of 10°. The experimental results for ^{27}Na are best reproduced with $\theta_R = 10°$ and a scaling factor of 0.11. This result is in agreement with the results from the reactions investigated by Okuno *et al.* [6] onto a light (^{27}Al) target. E.g., for ^{12}B fragments, produced with a ^{15}N beam ($\theta_L = 1.0(5)°$; $E = 68$ MeV/nucleon) the polarization was found to be a factor of 10 smaller than predicted by the model and an angle $\theta_R = 10°$ gave the best reproduction of the experimental trends as a function of p_f. Thus, the model is able to predict the trend of the polarization but overestimates the reaction-induced polarization on light targets by an order of magnitude, independent on how many nucleons are removed (here nine, in Ref. [6] three). Note that the evaporated nucleons are removed isotropically and spin polarization is created by the abraded nucleons (1 evaporated nucleon for 2 abraded nucleons is assumed in intermediate energy reactions). In Fig. 5(c) the theoretical polarization is compared for fragments with different mass A, all produced with ^{36}S projectiles at 77.5 MeV/nucleon onto a ^{9}Be target. The simulations are made for a reaction angle $\theta_R = 10°$. The polarization diminishes with an increasing number of removed nucleons. However, sufficient polarization remains, even if nine nucleons are removed such as for ^{27}Na. This is an indication that sufficient polarization can be produced, even for fragments differing significantly from the projectile nucleus. The curve of $A = 31$ in Fig. 5(c) corresponds also to the polarization we would expect for the ^{31}Al fragments, because the proton number Z of the fragments is not a parameter in the present kinematical fragmentation model. However, in our experimental data [Fig. 5(b)] we find less polarization. This is most likely due to additional orientation losses, what we represented in the formula of the reaction induced polarization by the factor q ($P_r = P/q$). The deduced polarization [Eq. (10)] is calculated from the observed β asymmetry, neglecting the unquantifiable orientation losses q. For the substitutionally implanted ^{27}Na in NaCl, where $q \simeq 1$, this is justified. In the case of ^{31}Al, the unknown implantation behavior of ^{31}Al in MgO makes it necessary to introduce this unknown reduction factor q. The very small amount of deduced ^{31}Al polarization [$P = -1.5(4)\%$] compared to the calculated reaction induced polarization $P_r = -7.7\%$ [Fig. 5(c)], is likely due to the fact that only 19(5)% of the ^{31}Al nuclei contribute to the NMR effect ($q = 0.19$). The remaining 81% of the nuclei do not undergo a normal Zeeman splitting, because their nearest neighbor lattice structure might be perturbed.

Notice that the energy of the projectile beam was kept constant at 77.5 MeV/nucleon in the experiments of this report. In order to probe the issue whether spin polarization can be produced also at much higher energies, we plot in Fig. 6 the results of calculations performed with the kinematical fragmentation model. These calculations reveal, as expected,

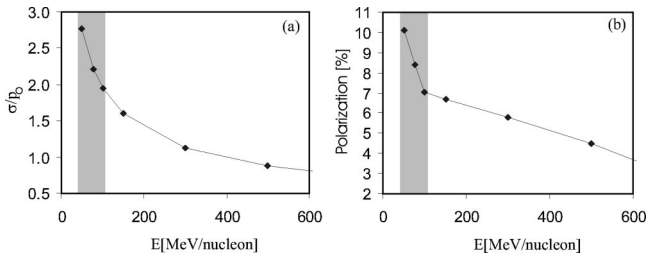

FIG. 6. Evolution of (a) the relative width σ/p_0 of the ^{27}Na linear fragment momentum distribution with increasing energy and (b) the polarization of ^{27}Na fragments, averaged over a momentum window of $p_f - p_0/p_0 = 0.3\%$ from the outer wing of the distribution. The beam deviation was taken as $\theta_L = -2(1)°$ and simulations are made for $\theta_R = 10°$ and a scaling factor of 0.11. The shaded region is the intermediate energy region for which experiments can be performed at GANIL.

a strong decrease of the relative width σ/p_0 of the fragment linear momentum distribution 6(a). Because a minimum linear momentum window is chosen with the momentum slits, the averaged polarization over such a momentum window will thus decrease as a function of the beam energy. Figure 6(b) shows the dependency on the beam energy of the polarization, averaged over a momentum window of $(p_f - p_0)/p_0 = 0.3\%$, starting from the outer wing at $(p_f - p_0)p_0 = \sigma/p_0$. Schäfer *et al.* [30] measured the polarization of ^{37}K , produced in a projectile-fragmentation reaction at 500 MeV/nucleon with ^{40}Ca projectiles on a ^{9}Be target. Fragments emitted at an angle of $-0.5(1)°$ were selected. A KBr crystal was used as a stopper. A more or less constant polarization of $P = -0.85(20)\%$ was deduced for different linear momentum selections spread over the whole momentum distribution. However the current model predicts a far-side-trajectory shape of the polarization as a function of the momentum distribution, with an averaged polarization over $(p - p_0)/p_0 = 0.3\%$ starting from the outer wing of $|P| = 7.8\%$. This indicates that the actual model does not reproduce the trend line and highly overestimates the polarization in high-energy projectile fragmentation reactions. In this regime, σ/p_0 approaches zero and the dominating process is not the deflection of fragments due to Coulomb and nuclear forces, but the straggling induced by the transverse momentum of the removed nucleons, which is neglected in the kinematical model of Okuno *et al.* Schäfer *et al.* [30] adapted the model for high energies, e.g., by taking into account this straggling.

VI. CONCLUSIONS

We have been able to produce spin-polarized fragments out of a reaction where a large number of nucleons was removed from the ^{36}S projectile nuclei. The deduced spin polarizations $P(^{27}\text{Na}) = -6.2(9)\%$ and $P(^{31}\text{Al}) = -1.5(4)\%$ will allow to investigate the moments of nuclei far from the valley of stability using spin-oriented beams at intermediate energies. The result for the ^{27}Na fragment nuclei indicates that high spin polarization can be produced also in projectile-fragmentation reactions where 25% of the

nucleons are removed from the projectile nucleus. The importance of this result is related to the possibility to study the structure of very exotic nuclei when going close to the dripline both at the proton- and neutron-rich side, also for heavier systems.

The knowledge of the experimentally obtained spin polarization is crucial to perform experiments in a confident way. The choice of the proper beam (isotope, energy) and target (material, thickness) combination is determinant for a good production rate and a reasonable spin polarization. Spin-polarization calculations using the kinematical fragmentation model of Okuno and co-workers [5,6] are reproducing the trends for the intermediate energy region, but have to be rescaled to experimental values by about a factor of 10 for reactions where the nuclear attraction is dominant (so on light targets). More experimental data are needed to understand fully the processes leading to spin orientation in a projectile-fragmentation reaction, especially at higher beam energy.

ACKNOWLEDGMENTS

We acknowledge support from the Access to Large Scale Facility program under the TMR program of the EU, under Contract No. HPRI-CT-1999-00019. Special thanks to H. Ogawa and K. Asahi for providing us the polarization code. G.N., K.V., and D.B. acknowledge the FWO-Vlaanderen for financial support. We are grateful for the technical support received from the staff of the GANIL facility. D.L.B. acknowledges a NATO research grant. M.H. acknowledges the support from the Israel Science Foundation (ISF).

[1] E. Arnold, J. Bonn, R. Gegenwart, W. Neu, R. Neugart, E.-W. Otten, G. Ulm, and K. Wendt, Phys. Lett. B **197**, 311 (1987).
[2] N. Severijns, J. Wouters, J. Vanhaverbeke, and L. Vanneste, Phys. Rev. Lett. **63**, 1050 (1989).
[3] G. Goldring, Hyperfine Interact. **75**, 355 (1992).
[4] M. Lindroos, C. Broude, G. Goldring, H. Haas, M. Hass, P. Richards, and L. Weissmann, Nucl. Instrum. Methods Phys. Res. A **362**, 53 (1995).
[5] K. Asahi, M. Ishihara, N. Inabe, T. Ichihara, T. Kubo, M. Adachi, H. Takanashi, M. Kouguchi, M. Fukuda, D. Mikolas, D.J. Morrissey, D. Beaumel, T. Shimoda, H. Miyatake, T. Takahashi, Phys. Lett. B **251**, 488 (1990).
[6] H. Okuno, K. Asahi, H. Sato, H. Ueno, J. Kura, M. Adachi, T. Nakamura, T. Kubo, N. Inabe, A. Yoshida, I. Ichihara, Y. Ohkubo, M. Iwamoto, F. Ambe, T. Shimoda, H. Miyatake, N. Takahasi, J. Nakamura, D. Beaumel, D.J. Morrissey, W.-D. Schmidt-Ott, and M. Ishihara, Phys. Lett. B **335**, 29 (1994).
[7] H. Okuno, K. Asahi, H. Ueno, H. Izumi, H. Sato, M. Adachi, T. Nakamura, T. Kubo, N. Inabe, A. Yoshida, T. Shimoda, H. Miyatake, N. Takahasi, W.-D. Schmidt-Ott, and M. Ishihara, Phys. Lett. B **354**, 41 (1995).
[8] H. Ueno, K. Asahi, H. Izumi, K. Nagata, H. Ogawa, A. Yoshimi, H. Sato, M. Adachi, Y. Hori, K. Mochinaga, H. Okuno, N. Aoi, M. Ishihara, A. Yoshida, G. Liu, T. Kubo, N. Fukunishi, T. Shimoda, H. Miyatake, M. Sasaki, T. Shirakura, N. Takahashi, S. Mitsuoka, and W.-D. Schmidt-Ott, Phys. Rev. C **53**, 2142 (1996).
[9] W.F. Rogers, G. Georgiev, G. Neyens, D. Borremans, N. Coulier, R. Coussement, A.D. Davies, J.L. Mitchell, S. Teughels, B.A. Brown, and P.F. Mantica, Phys. Rev. C **62**, 044312 (2000).
[10] E. Matthias, B. Olsen, D.A. Shirley, J.E. Templeton, and R.M. Steffen, Phys. Rev. A **4**, 1626 (1971).
[11] R. Anne and A.C. Mueller, Nucl. Instrum. Methods Phys. Res. B **70**, 276 (1992).
[12] A.S. Goldhaber, Phys. Lett. **53B**, 306 (1974).
[13] J. Hüfner and M.C. Nemes, Phys. Rev. C **23**, 2538 (1981).
[14] C.Y. Wong and K. Van Bibber, Phys. Rev. C **25**, 2990 (1982).
[15] W.A. Friedman, Phys. Rev. C **27**, 569 (1983).
[16] D. Bazin, O. Tarasov, M. Lewitowicz, O. Sorlin, Nucl. Instrum. Methods Phys. Res. A **482**, 307 (2002).
[17] http://www.ganil.fr/lise/proglise.html
[18] J.M. Daugas, R. Grzywacz, M. Lewitowicz, M.J. Lopez-Jimenez, F. de Oliveira-Santos, J.C. Angélique, L. Axelsson, C. Borcea, C. Longour, and G. Neyens, Phys. Rev. C **63**, 064609 (2001).
[19] D.J. Morrissey, Phys. Rev. C **39**, 460 (1989).
[20] N. Metropolis, R. Bivins, M. Storm, A. Turkevich, J.M. Miller, and G. Friedlander, Phys. Rev. **110**, 185 (1958).
[21] J.W. Negele and K. Yazaki, Phys. Rev. Lett. **47**, 71 (1981).
[22] D. Borremans, N.A. Smirnova, S. Teughels, L. Achouri, D.L. Balabanski, N. Coulier, J.-M. Daugas, G. de France, F. de Oliveira Santos, A. De Vismes, G. Georgiev, M. Lewitowicz, I. Matea, Yu. E. Penionzhkevich, P. Roussel-Chomaz, H. Savajols, W.-D. Schmidt-Ott, Yu. Sobolev, M. Stanoiu, O. Tarasov, K. Vyvey, and G. Neyens, Phys. Lett. B **537**, 45 (2002).
[23] *Low Temperature Nuclear Orientation*, edited by H. Postma and N. Stone (North-Holland, Amsterdam, 1986).
[24] Y. Yamazaki, O. Hashimoto, H. Ikezoe, S. Nagamiya, K. Nakai, and T. Yamazaki, Phys. Rev. Lett. **33**, 1614 (1974).
[25] P.M. Endt, Nucl. Phys. **A521**, 1 (1990).
[26] *Table of Isotopes*, 8th ed., edited by R.B. Firestone and V.S. Shirley (Wiley, New York, 1996), Vol. 1.
[27] GEANT Detector Description and Simulation Tool, http://www.info.cern.ch/asdoc/ geantold/geantmain.html
[28] G. Huber, F. Touchard, S. Bütchenbach, C. Thibault, R. Klapisch, H.T. Duong, P. Juncar, S. Liberman, J. Pinard, and J.L. Vialle, Phys. Rev. C **18**, 2342 (1978).
[29] S.K. Charagi and S.K. Gupta, Phys. Rev. C **41**, 1610 (1990).
[30] M. Schäfer, W.-D. Schmidt-Ott, T. Dörfler, T. Hild, T. Pfeiffer, R. Collatz, H. Geissel, M. Hellström, Z. Hu, H. Irnich, N. Iwasa, M. Pfützner, E. Roeckl, M. Shibata, B. Pfeiffer, K. Asahi, H. Izumi, H. Ogawa, H. Sato, H. Ueno, and H. Okuno, Phys. Rev. C **57**, 2205 (1998).